Title

Isocitrate Dehydrogenase Mutations Confer Dasatinib Hypersensitivity and SRC Dependence in Intrahepatic Cholangiocarcinoma

Journal

Cancer Discovery, 6(7)

ISSN

2159-8274

Authors

Saha, Supriya K
Gordan, John D
Kleinstiver, Benjamin P
et al.

Publication Date

2016-07-01

DOI

10.1158/2159-8290.cd-15-1442

Peer reviewed

Published in final edited form as:

Cancer Discov. 2016 July ; 6(7): 727–739. doi:10.1158/2159-8290.CD-15-1442.

Isocitrate dehydrogenase mutations confer dasatinib hypersensitivity and SRC-dependence in intrahepatic cholangiocarcinoma

Supriya K. Saha[1], **John D. Gordan**[2], **Benjamin P. Kleinstiver**[3,4], **Phuong Vu**[1], **Mortada S. Najem**[1], **Jia-Chi Yeo**[1], **Lei Shi**[1], **Yasutaka Kato**[1], **Rebecca S. Levin**[2], **James T. Webber**[2], **Leah J. Damon**[1], **Regina K. Egan**[1], **Patricia Greninger**[1], **Ultan McDermott**[5], **Mathew J. Garnett**[5], **Roger L. Jenkins**[6], **Kimberly M. Rieger-Christ**[7], **Travis B. Sullivan**[7], **Aram F. Hezel**[8], **Andrew S. Liss**[9], **Yusuke Mizukami**[1,10], **Lipika Goyal**[1], **Cristina R. Ferrone**[1], **Andrew X. Zhu**[1], **J. Keith Joung**[3,4], **Kevan M. Shokat**[11,12], **Cyril H. Benes**[1], and **Nabeel Bardeesy**[1]

[1]Massachusetts General Hospital Cancer Center, Harvard Medical School, Boston, MA 02114, USA

[2]Helen Diller Family Comprehensive Cancer Center, University of California, San Francisco, San Francisco, CA 94115, USA

[3]Molecular Pathology Unit, Center for Cancer Research, and Center for Computational and Integrative Biology, Massachusetts General Hospital, Charlestown, MA 02129

[4]Department of Pathology, Harvard Medical School, Boston, MA 02115, USA

[5]Wellcome Trust Sanger Institute, Hinxton, UK

[6]Department of Transplantation, Lahey Hospital and Medical Center, Burlington, MA, 01805, USA

[7]Department of Translational Research, Lahey Hospital and Medical Center, Burlington, MA, USA, 01805

[8]University of Rochester School of Medicine, Rochester, New York, 14642, USA

[9]Department of Surgery and the Andrew L. Warshaw, MD, Institute for Pancreatic Cancer Research, Massachusetts General Hospital and Harvard Medical School, Boston, Massachusetts, 02114, USA

[10]Center for Clinical and Biomedical Research, Sapporo Higashi Tokushukai Hospital, Sapporo, Hokkaido, Japan

[11]Department of Cellular and Molecular Pharmacology, University of California, San Francisco, San Francisco, CA 94158, USA

Corresponding Authors: Nabeel Bardeesy, 85 Cambridge St, CPZN 4216, Boston MA, 02114, Bardeesy.Nabeel@mgh.harvard.edu; Phone: 617-643-2579; Fax: 617-643-3170, Cyril Benes, CNY 149 Room 7401, 149 13th St, Charlestown, MA 02129, cbenes@mgh.harvard.edu, Phone: 617-724-3409, Fax: 617-726-7808.

Conflicts of Interest: J.K.J. is a consultant for Horizon Discovery. J.K.J. has financial interests in Editas Medicine, Hera Testing Laboratories, Poseida Therapeutics, and Transposagen Biopharmaceuticals. J.K.J.'s interests were reviewed and are managed by Massachusetts General Hospital and Partners HealthCare in accordance with their conflict of interest policies.

[12]Howard Hughes Medical Institute, University of California, San Francisco, San Francisco, CA 94158, USA

Abstract

Intrahepatic cholangiocarcinoma (ICC) is an aggressive liver bile duct malignancy exhibiting frequent isocitrate dehydrogenase (IDH1/IDH2) mutations. Through a high-throughput drug screen of a large panel of cancer cell lines including 17 biliary tract cancers, we found that IDH mutant (IDHm) ICC cells demonstrate a striking response to the multi-kinase inhibitor dasatinib, with the highest sensitivity among 682 solid tumor cell lines. Using unbiased proteomics to capture the activated kinome and CRISPR/Cas9-based genome editing to introduce dasatinib-resistant 'gatekeeper' mutant kinases, we identified SRC as a critical dasatinib target in IDHm ICC. Importantly, dasatinib-treated IDHm xenografts exhibited pronounced apoptosis and tumor regression. Our results show that IDHm ICC cells have a unique dependency on SRC and suggest that dasatinib may have therapeutic benefit against IDHm ICC. Moreover, these proteomic and genome-editing strategies provide a systematic and broadly applicable approach to define targets of kinase inhibitors underlying drug responsiveness.

Keywords

Mutant IDH; intrahepatic cholangiocarcinoma; dasatinib; high-throughput drug screen; biliary tract cancer

Introduction

Biliary tract cancers (BTCs) include a spectrum of invasive adenocarcinomas encompassing both cholangiocarcinoma arising in the intrahepatic, perihilar, or distal biliary tree, as well as carcinoma arising from the gallbladder (1). As a subset of BTCs, intrahepatic cholangiocarcinoma (ICC) is the second most common type of primary liver tumor, and has been rising in incidence worldwide for the past 3 decades (2). The reported incidence of ICC in the United States has risen from 0.44 per 100,000 in 1973 to 1.18 in 2012 (3), although the actual rate is likely significantly higher as recent molecular studies demonstrate that "carcinomas of unknown primary" are most commonly biliary in origin (4, 5). Despite the current standard chemotherapy with gemcitabine/cisplatin combination for patients with unresectable or metastatic BTCs, the median survival time remains less than one year (6), and there are no standard treatments for patients after progression on this regimen.

Recent work has provided a detailed view of the genetics of ICC (7–14), revealing that specific gain-of-function hot-spot mutations in IDH1 and IDH2 are among the most common genetic lesions in ICC (present in ~18–37% of ICC cases in North America and Europe). These mutations occur within the isocitrate binding site of IDH1 (R132) or IDH2 (R172, R140) and cause altered enzymatic function, leading to the production of *R*(–)-2-hydroxyglutarate (2HG), a proposed 'oncometabolite' (15). 2-HG inhibits members of the family of α-ketoglutarate-dependent dioxygenase enzymes, many of which function as epigenetic modifiers, resulting in genome-wide changes in the landscape of DNA and histone methylation marks (16–18). Mutant IDH impairs differentiation of a number of cell

lineages in a 2-HG-dependent manner. In the mouse liver, mutant IDH blocks adult liver progenitor cells from undergoing hepatocyte differentiation as an early event in ICC pathogenesis (19, 20). Accordingly, the IDHm subset of ICC has a distinct transcriptional signature compared to IDH wild-type (WT) tumors, characterized by enrichment of hepatic stem cell genes (19, 20).

There is a great deal of interest in the pharmacologic targeting of the mutant IDH enzyme and evidence of highly significant responses in acute myeloid leukemia patients treated with an IDH2 inhibitor (21). In advanced ICC, the role for mutant IDH remains unclear. Recently reported results from the ongoing phase I study of AG-120, the first-in-class IDH1 inhibitor, have demonstrated the potential for IDH inhibition to promote transient stabilization of disease in a subset of IDHm ICC patients (22); however, alternative or combinatorial strategies may be needed for durable remissions. Beyond inhibition of the mutant IDH enzyme, we hypothesized that the widespread changes in cell differentiation state, cell metabolism and epigenetic control provoked by IDH mutations (15) may confer additional vulnerabilities that can be targeted (23). We utilized a large scale high-throughput drug screen to uncover such synthetic lethal therapeutic interactions. Our results reveal that IDHm ICC represents a distinct subtype of ICC with a unique molecular signature and drug response profile. Most significantly, this approach revealed that IDHm cells were highly responsive to dasatinib, exhibiting the greatest sensitivity to this drug among all 682 solid tumor cell lines tested, which we demonstrated was due to a critical dependency on SRC signaling. Importantly, this potency corresponded to levels and duration of exposure which are readily attainable in the clinic, and, accordingly, dasatinib caused rapid and widespread cell death in IDHm patient-derived xenografts (PDXs). Thus, we have identified a novel and dramatic therapeutic vulnerability conferred by mutant IDH in ICC that has immediate translational potential.

Results

We assembled a collection of 17 BTC cell lines representing ICC, extrahepatic cholangiocarcinoma (ECC), and gallbladder cancer (GBC). Sequencing analysis identified two ICC cell lines with IDH1 mutations, RBE (R132S) and SNU-1079 (R132C). Neither cell line demonstrated specific sensitivity to the mutant IDH1 inhibitor, AGI-5027, compared to IDH WT ICC cell lines under normal *in vitro* growth conditions, despite effective reduction in 2HG levels (Supplementary Figure S1A–B). In order to identify alternative therapeutic strategies in this ICC subset, we subjected our BTC cell line collection to a high-throughput drug screen with 122 federal drug administration (FDA)-approved drugs or other clinically relevant compounds (Figure 1A and Supplementary Table S1). By quantifying the relative response to compounds targeting a wide range of pathways, this screen also allows us to generate a unique and functionally relevant drug sensitivity profile for each BTC cell line.

A broad range of responses to the different agents was observed across the cell line collection, with specific activity profiles for different BTC subtypes (Figure 1B, Supplementary Table S1). Notably, the two IDHm ICC cell lines segregated together in unbiased clustering analysis and apart from all the other BTC cell lines in the screen (Figure

1B and Supplementary Figure S2). Across the panel of drugs screened, the IDHm ICC lines were marked outliers in their response to the multi-tyrosine kinase inhibitor (TKI), dasatinib (Figure 1C). Most strikingly, when compared with a larger panel of 684 solid tumor cell lines screened in parallel, the IDHm ICC's ranked first and second in sensitivity (Figure 1D, x-axis: compare red dots and grey dots; Supplementary Table S2). The sensitivity of IDHm ICC was also among the top 8th percentile when compared to 201 hematopoietic cancer cell lines, with the small set of more responsive lines enriched for chronic myelogenous leukemias (CML) harboring BCR-ABL translocations, in keeping the inhibition of ABL activity by dasatinib and the highly effective clinical use of this drug in the treatment of translocation-positive CML (Figure 1D and Supplementary Table S2) (24, 25). Both IDHm ICC lines also demonstrated outlier sensitivity to saracatinib, a structurally unrelated TKI with an overlapping target profile (26, 27), suggesting a common mechanism of action (Figure 1D, y-axis; Supplementary Table S2). Thus, IDHm ICC cells show exceptional responsiveness to these inhibitors at a dose range suggesting potential clinical relevance.

We validated these findings in scaled up proliferation assays across our set of ICC cell lines and included the immortalized human cholangiocyte line, MMNK-1, as an additional reference. These studies confirmed that both RBE and SNU-1079 cells were highly sensitive to dasatinib (IC50 of 1 nM and 7 nM, respectively) compared to a panel of other human ICC cell lines and MMNK-1 cells (IC50 range of 29 – 562 nM) (Figure 2A, first panel, and Supplementary Table S3). We also confirmed the increased sensitivity of RBE and SNU-1079 cells to saracatinib relative to the IDH WT lines (Figure 2A). These responses did not reflect a general hypersensitivity to TKIs, since two other multi-TKIs with overlapping but distinct target profiles, bosutinib and ponatinib, were similarly potent against IDH WT and IDHm ICC cell lines (Figure 2A). To extend these findings, we generated a set of novel low passage human ICC cell lines from resected tumor specimens, which included an additional line harboring an endogenous IDH1 R132V mutation (designated ICC5). As with our established cell lines, ICC5 cells were highly and specifically responsive to dasatinib, with an IC50 of ~1nM versus, 175 nM and 87 nM in the IDH WT ICC1 and ICC2 lines, respectively (Figure 2B and Supplementary Table S3). Moreover, ICC5 showed sensitivity profiles that were comparable to our established IDH mutant ICC lines across each of the other three tyrosine kinase inhibitors, strongly suggesting that dasatinib and saracatinib target a common conserved dependency in this ICC subset (Figure 2B). Importantly, dasatinib induced rapid cell death specifically in IDHm ICC cell lines, as assessed by crystal violet staining and cleaved caspase-3 activity assays at 24 h (Supplementary Figure S3A and S3B). This pronounced sensitivity to dasatinib was not a general feature of IDH mutant cancers across different tissues, since cell lines derived from IDHm chondrosarcoma or lung adenocarcinoma (HT-1080, SW-1353, and COR-L105) were all relatively resistant when compared to IDHm ICC cells (IC50 = 1578 nM, 120.8 nM, and 43.5 nM, respectively) (Supplementary Figure S3C). Along these lines, IDHm ICC did not show differential sensitivity to agents reported to be selectively toxic to IDHm cancer cells from other tissues, including the BCL-2 inhibitor, ABT-199, and the NAMPT inhibitor, FK866, which were observed to have enhanced activity against IDHm leukemia and glioma, respectively (Supplementary Figure S3D and S3E) (28, 29). Thus, our data indicate that dasatinib has potent and specific synthetic lethal interactions with IDH mutations in ICC,

and that IDH mutant status is associated with distinct vulnerabilities in different cancer types.

The potency of dasatinib in patients with BCR-ABL-driven CML relates to rapid induction of apoptosis, since this drug has a relatively short serum half-life (~4 – 6 h) (24, 25). Thus, we next tested whether brief exposure to physiologically attainable concentrations of dasatinib induces lasting effects on IDHm ICC cells. SNU-1079 and MMNK-1 control cells were exposed to 100 nM dasatinib for 4 h and then switched to drug-free media for 48 h. Remarkably, this transient treatment induced profound lethality in IDHm ICC cells, with very few cells remaining after 48 h (Supplementary Figure S3F). We then extended our analysis of the correlation between IDH status and drug sensitivity profiles by comparing cell lines derived from genetically engineered mouse models of ICC harboring $IDH2^{R172K}$ and $Kras^{G12D}$ mutations (SS49 cells) or $Kras^{G12D}$ mutation and p53 deletion (425 and 537 cells) (20, 30). The IDHm ICC SS49 cells were highly sensitive to dasatinib (IC50 = 3.6 nM, versus > 100 nM in 425 and 537 cells) and to a lesser extent saracatinib, while the effects of bosutinib and ponatinib were comparable between genotypes, in line with the effects seen in human ICC cells (Figure 2C).

SS49 cells form robust tumors upon subcutaneous implant in SCID mice, enabling us to test the sensitivity of IDHm ICCs *in vivo*. Treatment with dasatinib (50 mg/kg daily) was initiated once tumors reached a volume of ~125 mm^3. Notably, dasatinib-treated tumors demonstrated rapid and sustained remission through two weeks of treatment (Figure 2D). Histologic analysis of tumors harvested after 2 days of dasatinib treatment revealed widespread necrotic tissue and activation of the apoptotic marker, cleaved-caspase 3, while vehicle-treated tumors were composed exclusively of viable ductal epithelia and stroma (Figure 2E). These effects were progressive, since residual tumors harvested after 14 days treatment exhibited increasing areas of hyalinized and necrotic tissue (Figure 2E). Finally, we developed a human PDX model (SS110) from a resected ICC harboring an IDH1 R132C mutation. Tumor fragments were passaged subcutaneously in immunocompromised mice and never adapted to tissue culture conditions. Established SS110 tumors (passage 2) were allowed to reach ~900 mm^3 and then treated with dasatinib for 7 days. Similar to our murine xenograft model, these PDX tumors responded by undergoing rapid and widespread necrosis (Figure 2F). By contrast, dasatinib had only minimal effects on the growth of an IDH WT ICC PDX (Supplementary Figure S3G and S3H). Thus, IDHm ICC cells demonstrate pronounced sensitivity to clinically relevant doses of dasatinib both *in vitro* and *in vivo*.

To gain insight into the mechanism underlying dasatinib sensitivity, we examined the impact of dasatinib on major oncogenic pathways in IDH WT and mutant ICC cells over a time-course of treatment. A series of key signaling networks, including the MAPK pathway (p-ERK1/2), the JAK/STAT pathway (pSTAT3), and pro/anti-apoptotic proteins (BCL-2, MCL-1, BIM, and PUMA), were all completely unaffected by cytotoxic concentrations of dasatinib over six hours of exposure (Figure 3A and data not shown). By contrast, markers of mTOR complex 1 (mTORC1) activation (p-p70S6K and p-S6) were potently inhibited between 1 and 6 h of treatment exclusively in IDHm cells, suggesting a genotype specificity of pathways downstream of dasatinib-targeted kinases in ICC (Figure 3A). Correspondingly, inhibition of mTOR with low concentrations of Torin 1 (5–25 nM) effectively reduced p-

p70S6K and p-S6 levels, and slowed cell proliferation of IDHm and IDH WT ICC cells (Supplementary Figure S4A–B), indicating that mTOR signaling supports the growth of all ICCs, and suggesting that specific control of mTORC1 downstream of dasatinib-targeted kinases contributes to the dasatinib sensitivity of IDHm cells.

We subsequently wished to determine the direct target(s) underlying the effect of dasatinib in IDHm ICC cells among the >40 kinases that are known to be inhibited by this drug at the dose range used in our studies (26, 31). First, we used a multiplexed inhibitor bead (MIB) column strategy in order to generate a comprehensive and unbiased list of active kinases that are inhibited by dasatinib in IDHm ICC cells (32, 33). In this approach, activated kinases in cell lysates are identified through their preferential binding to a column containing 12 kinase inhibitors coupled to sepharose beads. This allows broad capture of active kinases in untreated cells, and quantification of the targets of dasatinib by failure of the MIB column to capture kinases bound by dasatinib. After elution, kinases are identified by mass spectroscopy (MS) (Figure 3B). To characterize on-target effects in the active kinome, IDHm or WT ICC cells were treated with dasatinib or DMSO control for 1 h and the relative abundance of each active kinase was quantified by MIB followed by MS. We identified six kinases that were active at baseline and inhibited 75% or more in both IDHm ICC lines treated with dasatinib (Figure 3C and Supplementary Table S4). All of these kinases — SRC, YES1, LYN, DDR1, ABL1, and ABL2 — are known targets of dasatinib with IC50 values < 1 nM in cell-free assays (26).

To identify key targets among those identified by the MIB method we then turned to a genetic approach. The capacity of dasatinib to inhibit its targets is in part due to the insertion of the inhibitor in a hydrophobic pocket at the back of the ATP binding site. A threonine residue that allows access to this pocket has been designated as a ‘gatekeeper’ (34) whose mutation to a more bulky residue, such as isoleucine, leads to loss of inhibitor binding without affecting normal kinase activity (35). We therefore used CRISPR/Cas9 technology (36, 37) to screen for gatekeeper mutations that could rescue IDHm ICC cells from dasatinib-induced cytotoxicity. SNU-1709 cells were transfected with Cas9, a guide RNA targeting the endogenous *ABL1*, *ABL2*, *DDR1*, *LYN*, *YES1* or *SRC* loci, and a donor oligonucleotide encoding the appropriate gatekeeper mutation, and subsequently treated with dasatinib for 30 days (Figure 4A). Strikingly, the SRC gatekeeper mutation (SRC^{T341I}) fully rescued cell viability, resulting in the growth of dasatinib-resistant colonies, whereas none of the other guide RNAs conferred rescue (Figure 4B). We also failed to generate viable colonies using gatekeeper mutant guides for three additional dasatinib targets, FRK, CSK and EPHA4 (data not shown). Thus, our data show that SRC inhibition is critical for dasatinib-mediated cytotoxicity in IDH mutant ICC, although we cannot rule out additional targets that may contribute to this effect.

We confirmed that SNU-1079-SRC^{T341I} cells were highly resistant to dasatinib-induced cytotoxicity relative to the parental line (Figure 4C and D). Sequencing analysis demonstrated that the SNU-1079-SRC^{T341I} cells had the expected genomic editing of the *SRC* locus (Supplementary Figure S5A). In addition, whereas dasatinib fully inhibited SRC activity in the parental cells, as evidenced by loss of Y416 phosphorylation, the SRC^{T341I} cells were resistant (Figure 4E). Importantly, this was not unique to SNU-1079 cells, as

genome editing to introduce the SRC^{T341I} gatekeeper mutation into a second IDH mutant ICC cell line, RBE, also resulted in marked resistance to dasatinib (shifting IC50 >500 fold) (Figure 4F, top left panel, and Supplementary Figure S5B). In keeping with these results, gatekeeper mutant expression rescued the effect of dasatinib on key signaling pathways, with SRC^{T341I} cells maintaining phospho-p70S6K and phospho-S6 levels upon dasatinib treatment, in contrast to what is seen in parental cells (Figure 4G). Confirming the specificity of the rescue, SRC^{T341I} cells also showed increased resistance to saracatinib and bosutinib, but not ponatinib, which is designed to overcome this gatekeeper mutation (Figure 4F). In further validation studies, shRNA-mediated knockdown of SRC also reduced pS6 levels and abolished growth specifically in IDHm ICC cells (Supplementary Figure S5C and S5D). Thus, the potent cytotoxicity of dasatinib against IDHm ICC is due to the critical requirement for SRC tyrosine kinase activity in maintaining the growth and viability of these cells.

Discussion

ICC is a highly lethal malignancy with limited therapeutic options and no effective screening or prevention strategies. The discovery of frequent IDH mutations in ICC as well as in other cancers has lead to great enthusiasm for both unraveling their unusual effects on cancer cell biology and interrogating the mutant enzymes as drug targets. The development of potent, specific, and non-toxic mutant IDH inhibitors, and their effective deployment as single agents in IDHm leukemia represent important advances in oncology (21). Additionally, recent experimental studies have highlighted other potential synthetic lethal vulnerabilities in different IDHm cancers involving targeting the BET domain family of chromatin regulators, the BCL2 anti-apoptotic protein, and the mitochondrial NADH salvage pathway enzyme, NAMPT (28, 29, 38). Early preclinical work and clinical trials data indicate that mutant IDH inhibition may provide benefit in solid tumors, although the effects appear more modest than those seen in leukemia (22). Likewise, we did not observe outlier sensitivity in our human IDHm ICC cell lines to inhibitors of BCL2, NAMPT, or BET proteins (Supplementary Figure S3D, S3E and data not shown), suggesting that such vulnerabilities may be both genotype and cancer-specific.

Our studies were centered on utilizing an unbiased approach to identify FDA-approved or advanced clinical compounds that are effective against IDHm ICC. In addition to their therapeutic potential, these drugs can serve as functional probes to expose critical growth and survival pathways. However, the identification of the specific targets involved in the biologic response to these compounds is often a significant challenge. In the case of promiscuous multi-kinase inhibitors such as dasatinib, it can be particularly difficult to establish key targets mediating cytotoxicity when specific kinase driver mutations are absent. To address this, we used a comprehensive approach, employing a MIB column strategy to generate an unbiased list of likely targets, combined with CRISPR/Cas9-mediated genome editing to render the endogenous kinases resistant to dasatinib binding. These studies revealed that IDHm ICC have a pronounced and unexpected dependency on SRC signaling for cell growth and survival. We show that IDHm ICCs are profound outliers in their responsiveness to dasatinib, and that SRC gatekeeper mutants confer almost complete protection of these cells. Notably, although recognized as the first known

oncogene, there are surprisingly few examples of human cancers where endogenous SRC has been established to be critical for survival (39). These findings suggest a clinical path forward for the use of dasatinib or other SRC inhibitors in the treatment of IDHm ICC. Moreover, the methods used here provide a framework for the systematic identification of critical targets of kinase inhibitors in sensitive cancer cell lines.

Understanding the basis of the specific dasatinib hypersensitivity of IDHm ICC remains an important outstanding question. This effect does not appear to be associated with differences in overall SRC activity, since levels of SRC expression and activity did not correlate with dasatinib sensitivity or IDH status. In particular, SRC kinase activity was comparable in IDH WT and mutant cell lines (data not shown) and IDH WT and mutant ICCs in the TCGA database show similar SRC mRNA levels (data not shown). Nevertheless, there are marked distinctions in the downstream pathways controlled by SRC between IDHm and WT ICC (Figure 3A and Supplementary Figure S5C). It is noteworthy that all IDHm ICC models evaluated, including both human and murine cells harboring either IDH1 or IDH2 mutations, demonstrated a similar level of sensitivity to dasatinib. Yet, expression of mutant IDH alone is not sufficient to confer this response, as IDHm cells from other solid tumors (lung cancer and chondrosarcoma) had five- to 100-fold higher IC50 than IDHm ICC (Supplementary Figure S3C). Moreover, ectopic expression of mutant IDH only marginally increased the sensitivity of WT ICC cells (Supplementary Figure S6A–C). Thus, IDH mutations confer dasatinib hypersensitivity when present during ICC pathogenesis, but not when expressed exogenously in established tumors, which may reflect the unique selective pressures induced by these mutations or the 2HG oncometabolite during tumorigenesis. Accordingly, ICC tumors harboring endogenous IDH mutations define a distinct subtype of ICC, with a characteristic transcriptional and epigenetic profile (18, 20).

Rigorous preclinical and clinical studies will be required to determine the optimal strategy to exploit SRC inhibition in patients with IDHm ICC. As there is currently no standard second-line therapy, we have initiated a clinical trial to investigate the safety and efficacy of dasatinib in IDHm ICC patients who have progressed on chemotherapy. In addition, dasatinib could be used as an ‘anchor’ for exploring combinatorial strategies in IDHm ICC. The possible synergy of dasatinib with mutant IDH inhibitors, for instance, remains an active area of investigation. Unfortunately, our preliminary studies suggest that this combination may be antagonistic in some tumors, which implies a potential role for 2HG or mutant IDH enzymatic activity in maintaining dasatinib hypersensitivity (data not shown). Thus, an unbiased approach utilizing high-throughput combination drug screens may be needed to identify agents which synergize with dasatinib to further inhibit growth or enhance cell death in IDHm ICC.

Beyond targeting SRC in IDHm ICC, our approach provides a proof of principle for the use of high-throughput drug screening to identify novel drug efficacies in molecular subsets of BTC. In this regard, recent genetic studies have revealed a remarkable genetic heterogeneity in these diseases, with numerous recurrent mutations in epigenetic modifiers, receptor tyrosine kinases and tumor suppressor pathways (7–14). Here, we provide a database of the relative sensitivities of 17 BTC cell lines to 122 approved or advanced clinical compounds

as a resource (Supplementary Table S1), which may be used as a basis for additional translational studies linking genomic biomarkers to drug sensitivities.

Methods

Cell lines

Cell lines were obtained from the following sources: DSMZ (EGI-1), Riken Bioresource Center (HuCCT1, G-415, RBE, SSP-25, TFK-1, TGBC14TKB, YSCCC, TKKK, HuH-28), Korean Cell Line Bank (SNU-245, SNU-308, SNU-478, SNU-869, SNU-1079, SNU-1196), ATCC (HT-1080, SW-1353), and ECACC (COR-L105). CC-LP-1 and CC-SW-1 were kind gifts from Dr. PJ Bosma, SG231 from Dr. AJ Demetris, MMNK-1 from Dr. J Luyendyk, HKGZ-CC from Drs. XY Guan and S Ma. All cell lines were authenticated by STR DNA profiling the cell line bank from which they were obtained. Otherwise, CC-LP-1, CC-SW-1, SG231, HKGZ-CC, MMNK-1, ICC1, ICC2 and ICC5 were authenticated by STR DNA profiling through ATCC between December 2015 and March 2016. Additional information regarding culture conditions for all BTC cell lines are described in Supplementary Table S5. Information about cell lines used in the large cell line screen of dasatinib and saracatinib can be found in the high-throughput drug screen method section. Cell lines were grown at 37 °C under 5% CO2 in their required growth medium (Gibco) supplemented with 10% fetal bovine serum and 1% penicillin-streptomycin. To establish murine and human ICC cell lines, freshly isolated tumor specimens from $Kras^{G12D};IDH2^{R172K}$ (SS49) (20) or $Kras^{G12D};p53^{f/f}$ (537 and 425) (30) mice or ICC resection specimens, per our IRB-approved protocol (DFCI# 13-162), were minced with sterile razor blades, digested with trypsin for 30 mins at 37°C, and then resuspended in RPMI supplemented with 10% fetal bovine serum and 1% penicillin/streptomycin (Gibco #15140-122) for murine lines or RPMI supplemented with 20% fetal bovine serum, 1% L-glutamine (Gibco #25030-081), 1% MEM Non-Essential Amino Acids Solution (Gibco #11140-050), 1% Sodium Pyruvate (Gibco 11360-070), 0.5% penicillin/streptomycin, 10μg/mL gentamicin (Gibco #15710-064) and 0.2Units/mL human recombinant insulin (Gibco #12585-014) for human lines and seeded on plates coated with rat tail collagen (BD Biosciences). Cells were passaged by trypsinization, adapted to RPMI supplemented with 10% fetal bovine serum and 1% penicillin/streptomycin (human lines) and transferred to uncoated tissue culture plates prior to proliferation assays. All studies were done on cells cultivated for less than ten passages.

Mice and xenograft experiments

Mice were housed in pathogen-free animal facilities. All experiments were conducted under protocol 2005N000148 approved by the Subcommittee on Research Animal Care at Massachusetts General Hospital. For murine SS49 xenografts, $1x10^5$ cells were injected subcutaneously into the flanks of 6–8 week old female CB17/lcr-Prkdc^{scid}/lcrCr mice (561, Charles River). When tumors reached ~125 mm^3, mice were treated with either vehicle control or dasatinib 50 mg/kg daily by oral gavage. Tumor size was measured daily with a digital caliper. To develop an IDH mutant human PDX, we obtained tissue from a fresh resection specimen from a patient with an IDH1 R132C mutant ICC tumor, per our IRB-approved protocol (DFCI# 13–162). The tissue was rinsed in HBSS and cut into 0.3–0.5 mm^3 pieces with sterile razor blades. These tumor pieces were implanted subcutaneously

into 6–8 week old female NSG mice (NOD.Cg-*Prkdc*^{scid} *Il2rg*^{tm1Wjl}/SzJ, 00557, The Jackson Laboratory). Upon reaching ~900 mm^3, mice were randomized to either vehicle control or dasatinib 50 mg/kg daily by oral gavage for seven days prior to harvest.

High-throughput drug screen

High-throughput drug screening and sensitivity modeling (curve fitting and IC50 estimation) was performed essentially as described previously (40). All cell lines were sourced from commercial vendors except as indicated. Cells were grown in RPMI or DMEM/F12 medium supplemented with 5% FBS and penicillin/streptomycin, and maintained at 37°C in a humidified atmosphere at 5% CO2. Cell lines were propagated in these two media in order to minimize the potential effect of varying the media on sensitivity to therapeutic compounds in our assay, and to facilitate high-throughput screening. To exclude cross-contaminated or synonymous lines, a panel of 92 SNPs was profiled for each cell line (Sequenom, San Diego, CA) and a pair-wise comparison score calculated. In addition, short tandem repeat (STR) analysis (AmpFlSTR Identifiler, Applied Biosystems, Carlsbad, CA) was performed and matched to an existing STR profile generated by the providing repository. More information on the cell lines screened, including their SNP and STR profiles is available on the Genomics of Drug Sensitivity in Cancer project website (41). All drugs were sourced from Selleck Chemicals (Houston, USA) or provided by the laboratory of Nathanael Gray, Harvard Medical School after stringent quality control. This screen did not include AGI-5027 or other mutant IDH inhibitors. Briefly, cells were seeded at variable density to insure optimal proliferation during the assay. Drugs were added to the cells the day after seeding in 9 dose series with doses 2 fold apart covering a range of 256 fold. Concentrations were chosen as possible based on known in cell targeting to minimize off target effects. Viability was determined using either Syto60 or resazurin after 3 days of drug exposure as previously described (34). Figures 1B–C displaying drug response across the ICC lines were prepared using GENE-E (42).

Proliferation assays

Cells were plated in 96-well plates (1000 cells/well) in culture medium. The following day, increasing doses of either AGI-5027 (ML309) (43) (gift from Agios Pharmaceuticals), dasatinib (S1021, Selleck Chemicals, Houston, TX), saracatinib (S1006, Selleck Chemicals), bosutinib (S1014, Selleck Chemicals), ponatinib (S1490, Selleck Chemicals), Torin 1 (S2827, Slleck Chemicals), FK866 (S2799, Selleck Chemicals) or DMSO (BP231-100, Fisher Scientific) control was added and the cells were allowed to grow until DMSO-treated wells reached confluency (5–7 days). To quantify viable cells, MTT (3-(4,5-Dimethylthiazol-2-yl)-2,5-Diphenyltetrazolium Bromide (M-6494, ThermoFisher Scientific) was added to the culture media at a final concentration of 1 mg/mL and incubated for 3 h at 37°C. Formazan crystals were solubilized with 100 μL/well of DMSO and absorbance was read at 490 nm and normalized to DMSO control. MTT proliferation assays were performed in duplicate and data are represented as mean ± s.e.m. between three independent experiments unless otherwise indicated in the figure legend.

Constructs and Viral infection

Human IDH1^{R132C}, IDH2^{R172K} and pMSCV-blast constructs were described previously (20). The following lentiviral plasmids were used: Human shSRC #1 (TRCN0000195339) target sequence: 5′-CATCCTCAGGAACCAACAATT-3′; shSRC #2 (TRCN0000199186) target sequence: 5′-CTGACTGAGCTCACCACAAAG-3′; shSRC #3 (TRCN0000038150) target sequence: 5′-GACAGACCTGTCCTTCAAGAA-3′. pLKO.1 shRNA with target sequence 5′-GCAAGCTGACCCTGAAGTTCAT-3′ was used as negative control. Viral particles containing the above mentioned plasmids were synthesized using either lentiviral (pCMV-dR8.91) or retroviral (pCL-ECO) packaging plasmids with pCMV-VSV-G (Addgene). Cells were infected by incubating with virus and 8 μg/ml polybrene (Millipore, #TR-1003-G). Twenty-four hours later, cells were selected in 2.5 μg/ml puromycin for at least two days and the pooled populations were used for various experiments.

Immunoblot analysis

Cell extracts were prepared in 1x RIPA buffer (150 mM NaCl, 1% IGEPAL, 0.1% SDS, 50 mM Tris, 0.5% DOC) supplemented with a protease inhibitor cocktail (Complete, Roche Applied Science, Indianapolis, IN) and phosphatase inhibitors (Phosphatase Inhibitor Cocktail Sets I and II, Calbiochem, San Diego, CA) and quantified by BCA Protein Assay (Thermo Scientific, Rockford, IL). For detection of pSRC Y416, cells were first fractionated using a NE-PER Extraction kit (7833, Thermo Scientific experiments) per the manufacturer's recommended protocol, and the insoluble fraction is shown. 30 μg protein was resolved on 8–11% SDS-PAGE gels and transferred onto PVDF membranes (GE Healthcare Life Sciences, Pittsburgh, PA). Membranes were blocked in TBS with 5% non-fat milk and 0.1% Tween® 20 (BP 337–500, Fisher Scientific) and probed with antibodies against IDH1 (#3997S, Cell Signaling), IDH2 (NBP2-22166, Novus Biologicals), phospho-p70 S6 Kinase (Thr389) (#9234, Cell Signaling, Danvers, MA), total p70S6K (#2708, Cell Signaling), phospho-S6 (Ser235/236) (#4858, Cell Signaling), total S6 (#2217, Cell Signaling), phospho-ERK1/2 (Thr202/Tyr204) (#9101, Cell Signaling), total ERK1/2 (#4695, Cell Signaling), phosph-STAT3 (Ser727) (#9134, Cell Signaling), total STAT3 (#9139, Cell Signaling), BCL2 (#2872, Cell Signaling), MCL1 (sc-819, Santa Cruz Biotechnology, Dallas, TX), pSRC Y416 (#6943, Cell Signaling), total SRC (#2123, Cell Signaling), or ACTIN (A5316, Sigma-Aldrich, St. Louis, MO) as loading control. Bound proteins were detected with horseradish-peroxidase-conjugated secondary antibodies (Vector Biolaboratories, Burlingame, CA) and SuperSignal West Pico Luminol/Enhancer Solution (Thermo Scientific).

Multiplex inhibitor bead column

Kinase chromatography and mass spectrometry was performed as described previously (33). Briefly, compounds were commercially obtained or synthesized directly, and then affixed to sepharose using 1-Ethyl-3-(3-dimethylaminopropyl)carbodiimide (EDC)-catalyzed peptide coupling chemistry. Cell lysates were then diluted in binding buffer with 1M NaCl and affinity purification was performed with gravity chromatography. The bound kinases were stringently washed and then eluted with hot SDS before extraction and tryptic digest. Liquid chromatography-tandem mass spectrometry (LC MS/MS) was performed on a Velos

Orbitrap (Thermo) with in-line HPLC using an EASY-spray column (Thermo). Label-free quantification was performed with Skyline (44), and statistical analysis with Ms Stats (45).

Caspase 3/7 activity

Cells were plated at confluency (10,000 cells/well) and allowed to adhere for 24 h in 96-well plate format. The following day, the cells were treated with dasatinib 100 nM. After incubation with dasatinib for 24h, caspase 3/7 activity was assessed using a Caspase-Glo® 3/7 Assay (G8090, Promega) per the manufacturer's recommended protocol. Data are represented as mean ± s.d. between technical triplicates (Figure 2C) or duplicates (Figure 4D).

Crystal violet staining

Cells were plated at confluency in 24-well plates (100,000 cells/well) and allowed to adhere overnight. The following day, the cells were treated with DMSO or dasatinib 100 nM. 24 h later, the media was aspirated and cells were washed with PBS, prior to fixation with ice-cold methanol for 20 min. The cells were then stained with 0.5% crystal violet in 25% methanol for 20 min at room temperature. Next, crystal violet stain was aspirated and cells were rinsed in tap water until excess crystal violet stain was removed (~20min).

CRISPR/Cas9-mediated genome editing

Plasmids used in this study can be found in Supplementary Table S6, and the sequences of oligonucleotides can be found in Supplementary Table S7. Target kinase loci in RBE and SNU-1079 cells were sequenced to identify and account for any cell-type specific polymorphisms. To do so, the genomic sequence flanking the intended genome-editing alteration was amplified using Phusion Hot Start Flex DNA Polymerase (New England Biolabs) with the primers listed in Supplementary Table S7. The resulting PCR amplicons were cloned using the Zero Blunt TOPO PCR Cloning Kit (Invitrogen), transformed into E.coli XL-1 blue competent cells, and ~20–25 colonies were grown overnight at 37°C in TB media prior to miniprep (MGH DNA Core) and Sanger sequencing. Single guide-RNAs (sgRNAs) targeting the putative locations of kinase gatekeeper mutations were designed so that the SpCas9 binding site overlapped the desired change. Oligonucleotides corresponding to the spacer sequence of the target site (Supplementary Table S7) were annealed and ligated into BsmBI cut BPK1520 (46) to generate the final sgRNA plasmids. Donor oligonucleotides were designed to include the desired gatekeeper mutation, as well as non-synonymous changes to prevent re-cleavage of the corrected allele (Supplementary Table S7). Transfection conditions for both RBE and SNU-1079 cells were first optimized with the Cell Line Optimization Nucleofector™ Kit for Nucleofector™ Device (Lonza) and a Nucleofector™ 2b Device (Lonza) according to the manufacturer's recommended protocol. Using the Cell Line Nucelofector® Kit L (VVCA-1005, Lonza) and program A-020, 1.5 μg of Cas9 expression plasmid that encoded either wild-type SpCas9 (JDS246, (47)) or SpCas9-VQR (MSP469, (46)), 500 ng of sgRNA expression plasmid (Supplementary Table S6), and 150 pmol of donor oligonucleotide (Supplementary Table S7) were transfected for each individual kinase into 1 x 10^6 RBE or 2.5 x 10^6 SNU-1079 cells. Following transfection, the cells were split in to three separate wells on 6-well plates. Genome editing was allowed to proceed for three days, prior to treating the cells with dasatinib 50 nM for 30

days to select for dasatinib-resistant cells. Crystal violet staining of one of the three wells is shown in Figure 4B, while the second and third wells were used for confirmation of the appropriate SRC mutation and subsequent assays. Successful insertion of gatekeeper mutations in the endogenous *ABL1*, *ABL2*, *DDR1*, *LYN* and *YES1* loci was not confirmed as no viable colonies survived dasatinib selection. Control transfections without the donor oligonucleotide containing the gatekeeper mutation were performed in parallel and did not yield any resistant colonies for any of the kinases attempted (data not shown).

Histology and immunostaining

Tissue samples were fixed overnight in 4% buffered formaldehyde, and then embedded in paraffin and sectioned (5 μm thickness) by the DF/HCC Research Pathology Core. Hematoxylin & eosin staining was performed using standard methods. For immunohistochemistry, unstained slides were baked at 55°C overnight, deparaffinized in xylenes (2 treatments, 6 min each), rehydrated sequentially in ethanol (5 min in 100%, 3 min in 95%, 3 min in 75%, and 3 min in 40%), and washed for 5 min in 0.3% Triton X-100/PBS (PBST) and 3 min in water. For antigen unmasking, specimens were cooked in a 2100 Antigen Retriever (Aptum Biologics Ltd, Southampton, UK) in 1X Antigen Unmasking Solution, Citric Acid Based (H-3300, Vector Laboratories), rinsed 3 times with PBST, incubated for 10 min with 1% H_2O_2 at room temperature to block endogenous peroxidase activity, washed 3 times with PBST, and blocked with 5% goat serum in PBST for 1 h. Anti-Cleaved Caspase 3 (#9661, Cell Signaling) was diluted in blocking solution at a ratio of 1:300 and incubated with the tissue sections at 4°C overnight. Specimens were then washed three times for 3 min each in PBST and incubated with biotinylated secondary antibody (Vector Laboratories) in blocking solution for 1h at room temperature. Then, specimens were washed 3 times in PBST and treated with ABC reagent (Vectastain ABC kit #PK-6100) for 30 min, followed by three washes for 3 min each. Finally, slides were stained for peroxidase for 3 min with the DAB (Di-amine-benzidine) substrate kit (SK-4100, Vector Laboratories), washed with water and counterstained with hematoxylin. Stained slides were photographed with an Olympus DP72 microscope. Quantification of % necrosis in tumor slides was performed by a pathologist (Y.K.) who was blinded to the origin of the tissue. Data are represented as mean ± s.e.m.

2HG Measurements

Cells were seeded in 10 cm plates and grown to ~70% confluency. Media was then refreshed 3 hours prior to harvest. To extract intracellular metabolites, cells were briefly washed with ice-cold 0.9% sodium chloride, immediately fixed with chilled acetonitrile/methanol/water (40/40/20) and frozen in liquid nitrogen. Cells were then scraped, transferred into 1.5 mL eppendorf tubes, and vortexed. A series of 3 freeze/thaw cycles on dry ice were performed. The cellular lysate was clarified by centrifugation at 15,000 g at 4°C for 15 minutes. Clarified lysate was then directly analyzed by high performance liquid chromatography-mass spectrometry (HPLC-MS) as described previously (48).

Statistics

For studies following the high throughput screen, GI_{50} (defined as the concentration required to inhibit cell proliferation to 50% of untreated control) determinations were made

with GraphPad Prism software. A two-tailed Student's *t* test was used to assess significance for Caspase 3/7 activity assays, histological analysis of % tumor necrosis and the effect of SRC knockdown on proliferation. Analysis of variance (ANOVA) was used to analyze significance for the effect of dasatinib on SS49 xenograft growth. *P* values <0.05 were considered significant.

Supplementary Material

Refer to Web version on PubMed Central for supplementary material.

Acknowledgments

Financial Support: This work was supported by a Translational Research Award from the V Foundation to N.B., C.H.B., and A.X.Z and by a grant from TargetCancer Foundation to N.B. N.B. is the holder of the Gallagher Chair in Gastrointestinal Cancer Research at Massachusetts General Hospital. S.K.S. is supported by a NCI Mentored Clinical Scientist Research Career Development Award (1K08CA194268-01) and a DF/HCC GI SPORE Career Development Project Award (P50CA127003). J.D.G. was supported by an American Cancer Society Postdoctoral Grant. K.M.S. is a Howard Hughes Medical Institute Investigator. B.P.K. was supported by a Natural Sciences and Engineering Research Council of Canada Postdoctoral Fellowship. C.H.B, U.M. and M.J.G. are supported by a grant from the Wellcome Trust (102696). J.K.J. is supported by an NIH Director's Pioneer Award (DP1 GM105378) and is a consultant for Horizon Discovery. J.K.J. has financial interests in Editas Medicine, Hera Testing Laboratories, Poseida Therapeutics, and Transposagen Biopharmaceuticals. J.K.J.'s interests were reviewed and are managed by Massachusetts General Hospital and Partners HealthCare in accordance with their conflict of interest policies.

We thank Nathanael Gray, Harvard Medical School, for providing screening compounds, and members of the Bardeesy and Benes labs for helpful discussions.

References

1. Razumilava N, Gores GJ. Cholangiocarcinoma. Lancet. 2014; 383:2168–79. [PubMed: 24581682]
2. Khan SA, Thomas HC, Davidson BR, Taylor-Robinson SD. Cholangiocarcinoma. Lancet. 2005; 366:1303–14. [PubMed: 16214602]
3. Saha SK, Zhu AX, Fuchs CS, Brooks GA. Forty-Year Trends in Cholangiocarcinoma Incidence in the U.S.: Intrahepatic Disease on the Rise. The oncologist. 2016
4. Hainsworth JD, Rubin MS, Spigel DR, Boccia RV, Raby S, Quinn R, et al. Molecular gene expression profiling to predict the tissue of origin and direct site-specific therapy in patients with carcinoma of unknown primary site: a prospective trial of the Sarah Cannon research institute. Journal of clinical oncology : official journal of the American Society of Clinical Oncology. 2013; 31:217–23. [PubMed: 23032625]
5. Varadhachary GR, Raber MN. Cancer of unknown primary site. The New England journal of medicine. 2014; 371:757–65. [PubMed: 25140961]
6. Valle J, Wasan H, Palmer DH, Cunningham D, Anthoney A, Maraveyas A, et al. Cisplatin plus gemcitabine versus gemcitabine for biliary tract cancer. The New England journal of medicine. 2010; 362:1273–81. [PubMed: 20375404]
7. Borger DR, Tanabe KK, Fan KC, Lopez HU, Fantin VR, Straley KS, et al. Frequent mutation of isocitrate dehydrogenase (IDH)1 and IDH2 in cholangiocarcinoma identified through broad-based tumor genotyping. The oncologist. 2012; 17:72–9. [PubMed: 22180306]
8. Chan-On W, Nairismagi ML, Ong CK, Lim WK, Dima S, Pairojkul C, et al. Exome sequencing identifies distinct mutational patterns in liver fluke-related and non-infection-related bile duct cancers. Nature genetics. 2013; 45:1474–8. [PubMed: 24185513]
9. Jiao Y, Pawlik TM, Anders RA, Selaru FM, Streppel MM, Lucas DJ, et al. Exome sequencing identifies frequent inactivating mutations in BAP1, ARID1A and PBRM1 in intrahepatic cholangiocarcinomas. Nature genetics. 2013; 45:1470–3. [PubMed: 24185509]

10. Kipp BR, Voss JS, Kerr SE, Barr Fritcher EG, Graham RP, Zhang L, et al. Isocitrate dehydrogenase 1 and 2 mutations in cholangiocarcinoma. Human pathology. 2012; 43:1552–8. [PubMed: 22503487]
11. Ross JS, Wang K, Gay L, Al-Rohil R, Rand JV, Jones DM, et al. New routes to targeted therapy of intrahepatic cholangiocarcinomas revealed by next-generation sequencing. The oncologist. 2014; 19:235–42. [PubMed: 24563076]
12. Sia D, Losic B, Moeini A, Cabellos L, Hao K, Revill K, et al. Massive parallel sequencing uncovers actionable FGFR2-PPHLN1 fusion and ARAF mutations in intrahepatic cholangiocarcinoma. Nature communications. 2015; 6:6087.
13. Voss JS, Holtegaard LM, Kerr SE, Fritcher EG, Roberts LR, Gores GJ, et al. Molecular profiling of cholangiocarcinoma shows potential for targeted therapy treatment decisions. Human pathology. 2013; 44:1216–22. [PubMed: 23391413]
14. Wang P, Dong Q, Zhang C, Kuan PF, Liu Y, Jeck WR, et al. Mutations in isocitrate dehydrogenase 1 and 2 occur frequently in intrahepatic cholangiocarcinomas and share hypermethylation targets with glioblastomas. Oncogene. 2012
15. Cairns RA, Mak TW. Oncogenic isocitrate dehydrogenase mutations: mechanisms, models, and clinical opportunities. Cancer discovery. 2013; 3:730–41. [PubMed: 23796461]
16. Lu C, Ward PS, Kapoor GS, Rohle D, Turcan S, Abdel-Wahab O, et al. IDH mutation impairs histone demethylation and results in a block to cell differentiation. Nature. 2012; 483:474–8. [PubMed: 22343901]
17. Turcan S, Rohle D, Goenka A, Walsh LA, Fang F, Yilmaz E, et al. IDH1 mutation is sufficient to establish the glioma hypermethylator phenotype. Nature. 2012; 483:479–83. [PubMed: 22343889]
18. Wang P, Dong Q, Zhang C, Kuan PF, Liu Y, Jeck WR, et al. Mutations in isocitrate dehydrogenase 1 and 2 occur frequently in intrahepatic cholangiocarcinomas and share hypermethylation targets with glioblastomas. Oncogene. 2013; 32:3091–100. [PubMed: 22824796]
19. Saha SK, Parachoniak CA, Bardeesy N. IDH mutations in liver cell plasticity and biliary cancer. Cell cycle. 2014; 13:3176–82. [PubMed: 25485496]
20. Saha SK, Parachoniak CA, Ghanta KS, Fitamant J, Ross KN, Najem MS, et al. Mutant IDH inhibits HNF-4alpha to block hepatocyte differentiation and promote biliary cancer. Nature. 2014; 513:110–4. [PubMed: 25043045]
21. Stein E, Tallman M, Pollyea DA, Flinn IW, Fathi AT, Stone RM, et al. Abstract CT103: Clinical safety and activity in a phase I trial of AG-221, a first in class, potent inhibitor of the IDH2-mutant protein, in patients with IDH2 mutant positive advanced hematologic malignancies. Cancer Research. 2014; 74:CT103–CT103.
22. Burris H, Mellinghoff I, Maher E, Wen P, Beeram M, Touat M, et al. Abstract PL04-05: The first reported results of AG-120, a first-in-class, potent inhibitor of the IDH1 mutant protein, in a Phase I study of patients with advanced IDH1-mutant solid tumors, including gliomas. Molecular Cancer Therapeutics. 2015; 14:PL04–05.
23. Luo J, Solimini NL, Elledge SJ. Principles of cancer therapy: oncogene and non-oncogene addiction. Cell. 2009; 136:823–37. [PubMed: 19269363]
24. Shah NP, Kasap C, Weier C, Balbas M, Nicoll JM, Bleickardt E, et al. Transient potent BCR-ABL inhibition is sufficient to commit chronic myeloid leukemia cells irreversibly to apoptosis. Cancer cell. 2008; 14:485–93. [PubMed: 19061839]
25. Shah NP, Kim DW, Kantarjian H, Rousselot P, Llacer PE, Enrico A, et al. Potent, transient inhibition of BCR-ABL with dasatinib 100 mg daily achieves rapid and durable cytogenetic responses and high transformation-free survival rates in chronic phase chronic myeloid leukemia patients with resistance, suboptimal response or intolerance to imatinib. Haematologica. 2010; 95:232–40. [PubMed: 20139391]
26. Davis MI, Hunt JP, Herrgard S, Ciceri P, Wodicka LM, Pallares G, et al. Comprehensive analysis of kinase inhibitor selectivity. Nature biotechnology. 2011; 29:1046–51.
27. Green TP, Fennell M, Whittaker R, Curwen J, Jacobs V, Allen J, et al. Preclinical anticancer activity of the potent, oral Src inhibitor AZD0530. Molecular oncology. 2009; 3:248–61. [PubMed: 19393585]

28. Chan SM, Thomas D, Corces-Zimmerman MR, Xavy S, Rastogi S, Hong WJ, et al. Isocitrate dehydrogenase 1 and 2 mutations induce BCL-2 dependence in acute myeloid leukemia. Nature medicine. 2015; 21:178–84.
29. Tateishi K, Wakimoto H, Iafrate AJ, Tanaka S, Loebel F, Lelic N, et al. Extreme Vulnerability of IDH1 Mutant Cancers to NAD+ Depletion. Cancer cell. 2015; 28:773–84. [PubMed: 26678339]
30. O'Dell MR, Huang JL, Whitney-Miller CL, Deshpande V, Rothberg P, Grose V, et al. Kras(G12D) and p53 mutation cause primary intrahepatic cholangiocarcinoma. Cancer research. 2012; 72:1557–67. [PubMed: 22266220]
31. Karaman MW, Herrgard S, Treiber DK, Gallant P, Atteridge CE, Campbell BT, et al. A quantitative analysis of kinase inhibitor selectivity. Nature biotechnology. 2008; 26:127–32.
32. Duncan JS, Whittle MC, Nakamura K, Abell AN, Midland AA, Zawistowski JS, et al. Dynamic reprogramming of the kinome in response to targeted MEK inhibition in triple-negative breast cancer. Cell. 2012; 149:307–21. [PubMed: 22500798]
33. Sos ML, Levin RS, Gordan JD, Oses-Prieto JA, Webber JT, Salt M, et al. Oncogene mimicry as a mechanism of primary resistance to BRAF inhibitors. Cell reports. 2014; 8:1037–48. [PubMed: 25127139]
34. Liu Y, Shah K, Yang F, Witucki L, Shokat KM. A molecular gate which controls unnatural ATP analogue recognition by the tyrosine kinase v-Src. Bioorganic & medicinal chemistry. 1998; 6:1219–26. [PubMed: 9784863]
35. Daub H, Specht K, Ullrich A. Strategies to overcome resistance to targeted protein kinase inhibitors. Nature reviews Drug discovery. 2004; 3:1001–10. [PubMed: 15573099]
36. Hsu PD, Lander ES, Zhang F. Development and applications of CRISPR-Cas9 for genome engineering. Cell. 2014; 157:1262–78. [PubMed: 24906146]
37. Sander JD, Joung JK. CRISPR-Cas systems for editing, regulating and targeting genomes. Nature biotechnology. 2014; 32:347–55.
38. Chen C, Liu Y, Lu C, Cross JR, Morris JPt, Shroff AS, et al. Cancer-associated IDH2 mutants drive an acute myeloid leukemia that is susceptible to Brd4 inhibition. Genes & development. 2013; 27:1974–85. [PubMed: 24065765]
39. Brunton VG, Frame MC. Src and focal adhesion kinase as therapeutic targets in cancer. Current opinion in pharmacology. 2008; 8:427–32. [PubMed: 18625340]
40. Garnett MJ, Edelman EJ, Heidorn SJ, Greenman CD, Dastur A, Lau KW, et al. Systematic identification of genomic markers of drug sensitivity in cancer cells. Nature. 2012; 483:570–5. [PubMed: 22460902]
41. http://www.cancerRxgene.org
42. http://www.broadinstitute.org/cancer/software/GENE-E/
43. Davis MI, Gross S, Shen M, Straley KS, Pragani R, Lea WA, et al. Biochemical, cellular, and biophysical characterization of a potent inhibitor of mutant isocitrate dehydrogenase IDH1. The Journal of biological chemistry. 2014; 289:13717–25. [PubMed: 24668804]
44. Schilling B, Rardin MJ, MacLean BX, Zawadzka AM, Frewen BE, Cusack MP, et al. Platform-independent and label-free quantitation of proteomic data using MS1 extracted ion chromatograms in skyline: application to protein acetylation and phosphorylation. Molecular & cellular proteomics : MCP. 2012; 11:202–14. [PubMed: 22454539]
45. Choi M, Chang CY, Clough T, Broudy D, Killeen T, MacLean B, et al. MSstats: an R package for statistical analysis of quantitative mass spectrometry-based proteomic experiments. Bioinformatics. 2014; 30:2524–6. [PubMed: 24794931]
46. Kleinstiver BP, Prew MS, Tsai SQ, Topkar VV, Nguyen NT, Zheng Z, et al. Engineered CRISPR-Cas9 nucleases with altered PAM specificities. Nature. 2015; 523:481–5. [PubMed: 26098369]
47. Fu Y, Foden JA, Khayter C, Maeder ML, Reyon D, Joung JK, et al. High-frequency off-target mutagenesis induced by CRISPR-Cas nucleases in human cells. Nature biotechnology. 2013; 31:822–6.
48. Nicolay BN, Danielian PS, Kottakis F, Lapek JD Jr, Sanidas I, Miles WO, et al. Proteomic analysis of pRb loss highlights a signature of decreased mitochondrial oxidative phosphorylation. Genes & development. 2015; 29:1875–89. [PubMed: 26314710]

Significance

IDH mutations define a distinct subtype of intrahepatic cholangiocarcinoma (ICC), a malignancy that is largely refractory to current therapies. Our work demonstrates that IDH mutant ICC cells are hypersensitive to dasatinib and critically dependent on SRC activity for survival and proliferation, pointing to new therapeutic strategies against these cancers.

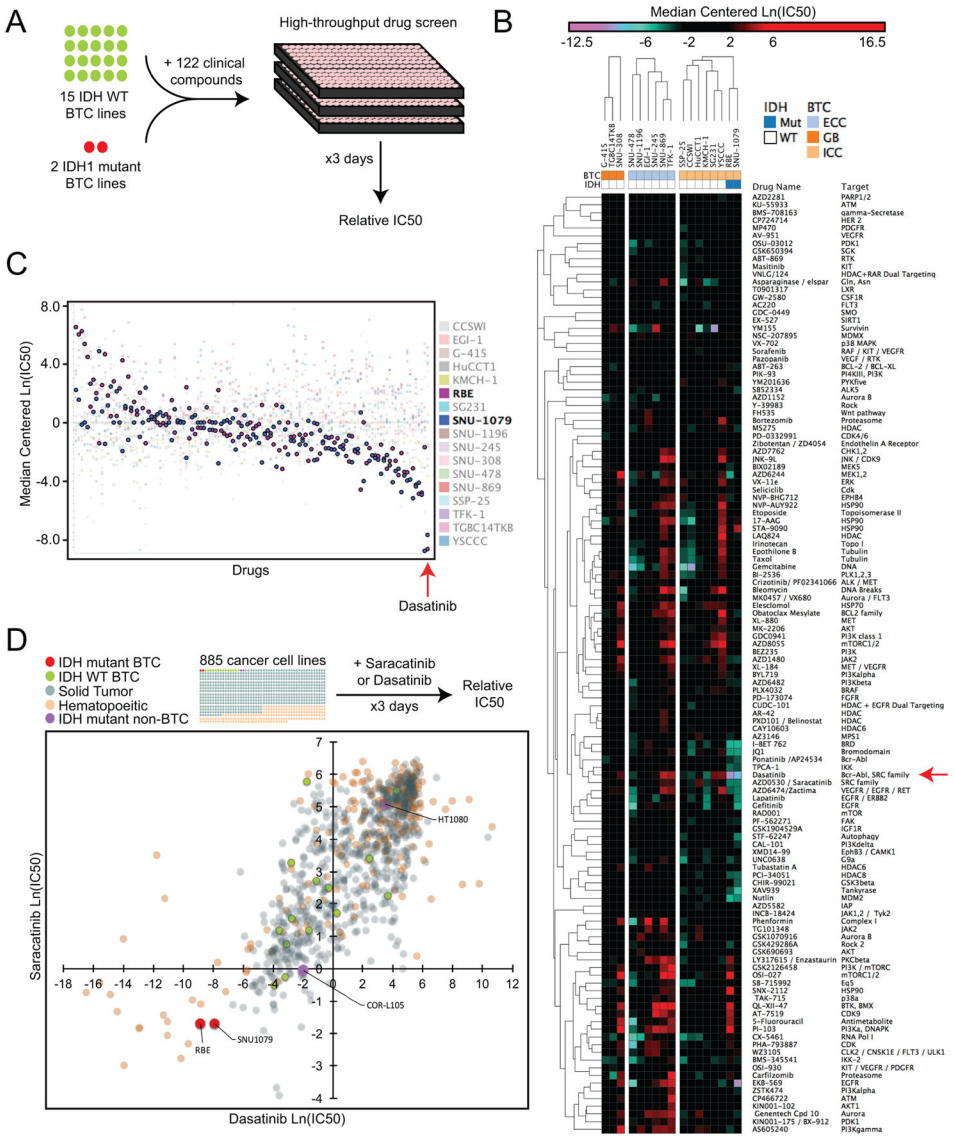

Figure 1. Isocitrate dehydrogenase (IDH) mutant intrahepatic cholangiocarcinoma (ICC) cells are hypersensitive to dasatinib

A. Schematic of the high-throughput drug screen protocol. 15 IDH wild-type (WT) biliary tract cancer (BTC) and two IDH mutant (IDHm) ICC cell lines were screened across 122 approved or advanced clinical compounds at nine different doses. Viability was quantified at 72 h and the IC50 estimated for each compound and cell line.

B. Heat map illustrating the median-centered Ln(IC50) of 17 BTC cell lines screened across 122 clinically relevant compounds. Note: the two IDH mutant (IDHm) ICC lines segregate together in unbiased hierarchical clustering.

C. Relative sensitivity (y-axis natural log scale, 0 = median Ln(IC50) across all BTC tested) of two IDHm ICC lines to 122 individual drugs (ranked by average sensitivity of IDHm ICC, x-axis). Note: Dasatinib demonstrates the greatest selective activity against IDHm ICC among drugs screened.

D. Sensitivity of 885 cancer cell lines to dasatinib (x-axis) and saracatinib (y-axis), each represented by an individual dot. IDHm ICC lines, RBE (IDH1 R132S) and SNU-1079 (IDH1 R132C) are the two larger red dots. IDHm non-BTC cell lines, HT1080 (IDH1 R132C) and COR-L105 (IDH1 R132C), are represented by purple dots. Drug response is presented as the natural logarithm of the IC50 in μM.

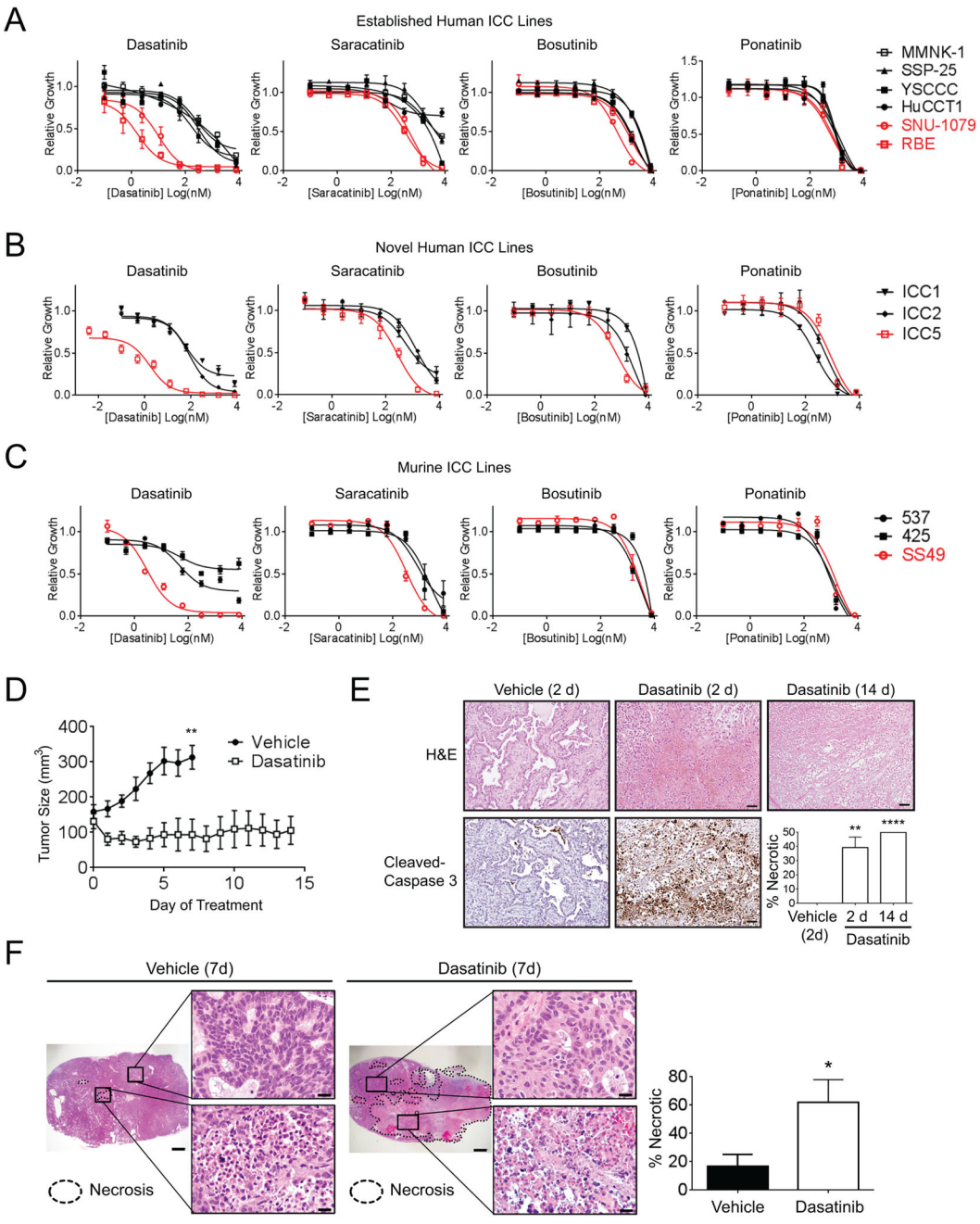

Figure 2. *In vitro* and *In vivo* hypersensitivity of IDHm ICC to dasatinib

A–C. Proliferation curves of established human (A), novel human (B) and murine (C) IDHm (red) and WT (black) ICC lines and MMNK-1 cells treated with increasing doses of the tyrosine kinase inhibitors, dasatinib, saracatinib, bosutinib and ponatinib.

D, E. Tumors arising from subcutaneously implanted murine IDHm ICC (SS49) cells were treated with either vehicle control or dasatinib 50 mg/kg daily by oral gavage. **D.** Serial tumor size measurements. **E.** Histologic analysis and immunostaining at the indicated time points revealed that dasatinib treatment causes widespread necrosis and activation of apoptotic markers. *Top panels*: H&E stain; *Bottom panels*: immunohistochemistry for

cleaved-caspase 3; inset: quantification of % necrotic tumor for vehicle (n = 3) or dasatinib treatment (n = 7 at 2 days, n = 5 at 14 days). Scale bars = 50 μm.

F. Histologic analysis (H&E) of an IDH1 R132C ICC patient-derived xenograft (PDX) treated with vehicle control or dasatinib 50mg/kg daily by oral gavage for seven days. *Right panel*: quantification of % necrotic tumor for vehicle (n = 5) and dasatinib treatment (n = 5). Scale bars = 1 mm (low power images) or 20μm (high power images). *p < 0.05, **p < 0.01, ****p<0.0001.

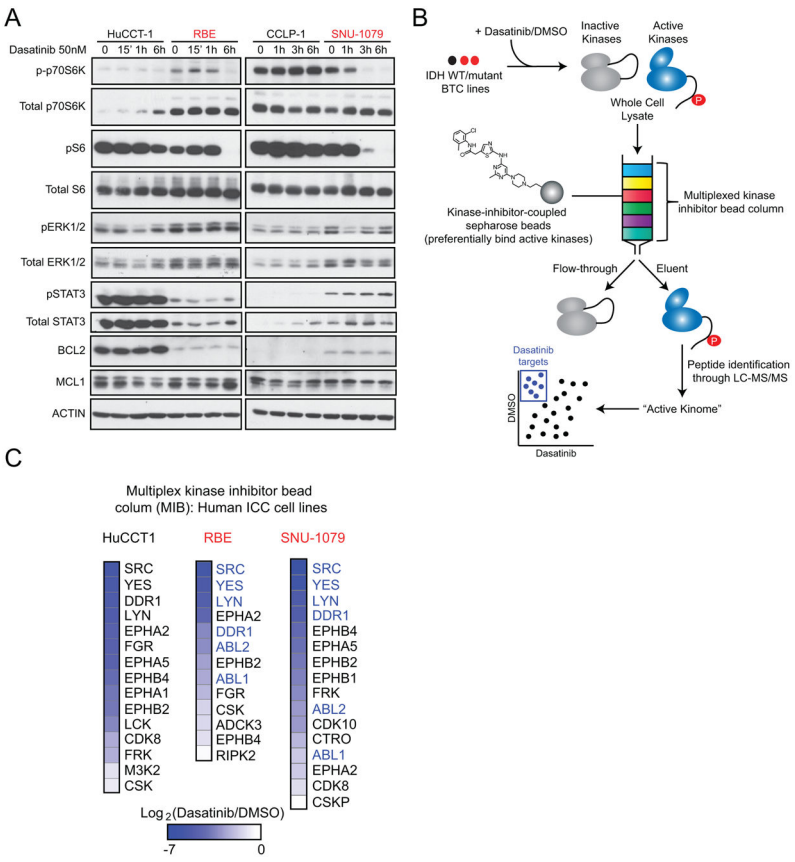

Figure 3. Identification of dasatinib targets in IDHm ICC

A. Immunoblot demonstrating that dasatinib causes loss of phospho-p70 S6 Kinase (Thr389) and phospho-S6 (Ser235/236) specifically in IDHm ICC cells. Neither IDHm nor IDH WT ICC show dasatinib-induced changes in phospho-ERK1/2 (Thr202/Tyr204), phosph-STAT3 (Ser727), BCL2, or MCL1.

B. Schematic illustrating methods used to characterize dynamic changes in the "active kinome" of ICC cells treated with dasatinib. IDH WT or IDHm ICC lines were treated with dasatinib (20 nM) or vehicle control for one hour prior to harvest. Whole cell lysates were run over a multiplexed kinase inhibitor bead (MIB) column containing a panel of sepharose beads covalently linked to 12 kinase inhibitors with distinct specificity profiles. Due to their preferential binding to active kinases, inactive kinases are discarded in the flow-through while active kinases were isolated in the eluent. The eluent was then subjected to tryptic digestion and peptide identification through liquid chromatography-tandem mass spectrometry (LC-MS/MS). To identify active kinases potently inhibited by dasatinib in each cell line, the active kinome of dasatinib-treated cells was compared to that of vehicle control.

C. Heat map of kinases enriched in the active kinome of dasatinib-treated cells compared to vehicle control cells (log_2 ratio is shown). Kinases that are active at baseline, inhibited >75% by dasatinib, and are common to both IDHm ICC are in blue.

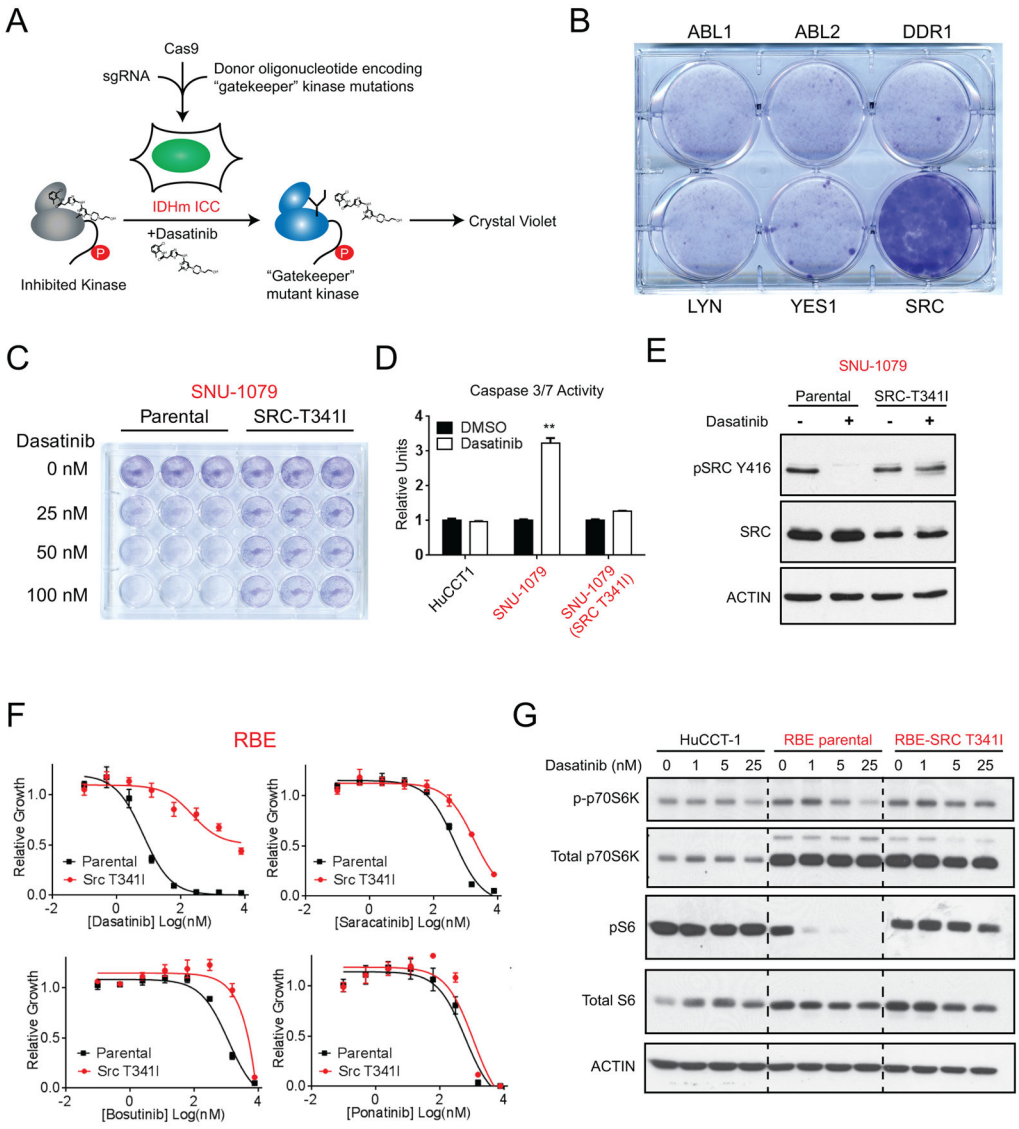

Figure 4. SRC is a critical dasatinib target in IDHm ICC

A. Schematic for the introduction of "gatekeeper" mutants into the endogenous loci encoding dasatinib targets in IDHm ICC cells. Plasmids containing Cas9 and a single guide RNA (sgRNA) targeting each individual kinase were co-transfected with a donor oligonucleotide encoding the gatekeeper mutation for each kinase. The gatekeeper mutation prevents the endogenously-expressed kinase from binding to and being inhibited by dasatinib, thus allowing dasatinib targets to remain active. Cells were then plated at confluency and treated with dasatinib 50 nM for 30 days in a six well plate.

B. Crystal violet staining of viable cells treated as in (A), demonstrating that introduction of the SRC T341I gatekeeper mutation rescues SNU-1079 cells from dasatinib-induced cytotoxicity.

C. Crystal violet stain of SNU-1079 parental cells and cells harboring an endogenous SRC-T341I mutation following treatment with increasing doses of dasatinib or DMSO control (0 nM) for 24 h.

D. Caspase 3/7 activity of HuCCT1 cells, SNU-1079 parental cells and SNU-1079-SRC T341I cells treated with dasatinib 100 nM for 24 h relative to DMSO control. **p<0.01.

E. Dasatinib treatment (50 nM) for 2 h causes loss of phospho-SRC (Tyr416) in parental SNU-1079 cells but not in SNU-1079-SRC T341I cells as shown by immunoblot of insoluble fractions.

F. Proliferation curves of RBE parental (black) or SRC-T341I (red) treated with increasing doses of dasatinib, saracatinib, bosutinib and ponatinib.

G. Immunoblot of lysates from RBE parental and SRC-T341I cells showing that the SRC gatekeeper mutation rescues phospho-p70 S6 Kinase (Thr389) and phospho-S6 (Ser235/236) levels in dasatinib-treated cells.